UNIVERSITY OF OKLAHOMA

GRADUATE COLLEGE

Searching for Supersymmetric Particles at the Large Hadron Collider using the ATLAS Detector

A DISSERTATION

SUBMITTED TO THE GRADUATE FACULTY

in partial fulfillment of the requirements for the

Degree of

DOCTOR OF PHILOSOPHY

By

OTHMANE RIFKI
Norman, Oklahoma
2016

Searching for Supersymmetric Particles at the Large Hadron Collider using the ATLAS Detector

A DISSERTATION APPROVED FOR THE
HOMER L. DODGE DEPARTMENT OF PHYSICS AND
ASTRONOMY

BY

Dr. Brad Abbott, Chair

Dr. Peter Parker, Outside Member

Dr. Mike Strauss

Dr. Chung Kao

Dr. Eric Abraham

To my loving parents and sister.

Table of Contents

Acknowledgements

I would like to acknowledge...

Abstract

Well now this is my abstract.

Preface

Chapter 1

Introduction

Chapter 2

Theoretical Background

2.1 The Standard Model of Particle Physics

2.2 Supersymmetry

2.3 Phenomenology at the LHC

Chapter 3

Experimental Apparatus

3.1 The Large Hadron Collider

3.2 A Toroidal LHC Apparatus (ATLAS)

3.3 ATLAS Detector

3.4 ATLAS Trigger and Data Acquisition System

3.5 Event Simulation

3.6 Reconstruction and Identification Techniques

Chapter 4

The Region of Interest Builder

4.1 Overview

4.2 VMEbus based RoIB

4.3 PC based RoIB

4.4 Prototype Tests

4.5 Online Performance in Run-2

4.6 Conclusion

Chapter 5

Analysis Strategy

5.1 Overview

5.2 Phenomenology (Benchmarking Models)

Final states with two same-sign leptons or three leptons and multiple jets can probe a variety of supersymmetric models represented by decays of heavy superpartners involving massive gauge bosons, sleptons or top quarks. The decays of the superpartners can lead to many experimental signatures that may lead to different lepton, jet, and b-tagged jet multiplicities. To exploit this wide range of possible signatures, the analysis uses six R-parity-conserving SUSY scenarios featuring gluino, bottom squark or top squark pair production. These scenarios were used as benchmarks to identify regions of the phase space where the analysis can bring particularly useful complementarity to other SUSY searches, and subsequently define signal regions with a particular focus on these regions. In this section, the scenarios considered are presetend with details about the assumed superpartner masses and decay modes. Exclusion limits obtained prior to the work of the author will also be shown to highlight the improvement in reach that this analysis brings.

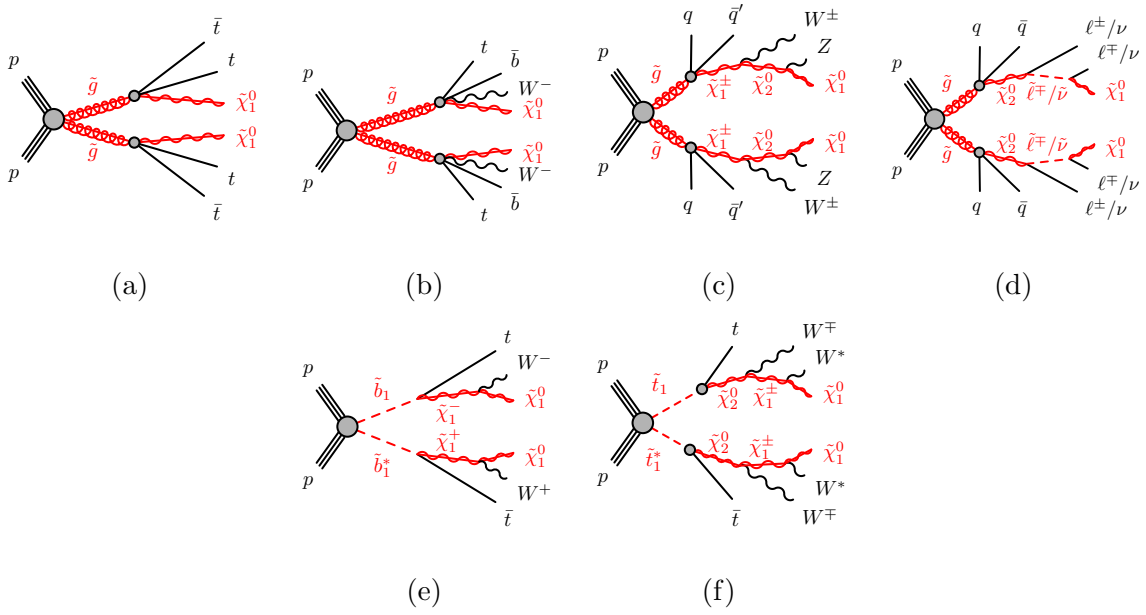

Figure 5.1: SUSY processes featuring gluino ((a), (b), (c), (d)) or third-generation squark ((e), (f)) pair production studied in this analysis. In Figure 5.1d, $\tilde{\ell} \equiv \tilde{e}, \tilde{\mu}, \tilde{\tau}$ and $\tilde{\nu} \equiv \tilde{\nu}_e, \tilde{\nu}_\mu, \tilde{\nu}_\tau$. In Figure 5.1f, the W^* labels indicate largely off-shell W bosons – the mass difference between $\tilde{\chi}_1^\pm$ and $\tilde{\chi}_1^0$ is around 1 GeV.

Gluino pair production with slepton-mediated two-step decay $\tilde{g} \to q\bar{q}\ell\bar{\ell}\tilde{\chi}_1^0$

This scenario (Fig. 5.1d) features gluino pair-production with two-step decays via neutralinos $\tilde{\chi}_2^0$ and sleptons, $\tilde{g} \to q\bar{q}'\tilde{\chi}_2^0 \to q\bar{q}'(\tilde{\ell}\ell/\tilde{\nu}\nu) \to q\bar{q}'(\ell\ell/\nu\nu)\tilde{\chi}_1^0$. The decays are mediated by generic heavy squarks, therefore the b-jet multiplicity in this scenario is low. The final state is made of charged leptons, four additional jets and invisible particles (neutrinos and neutralinos). The average jet multiplicity per event is the smallest among the four scenarios; another characteristic is the large fraction of events with several leptons, unlike the other scenarios that have

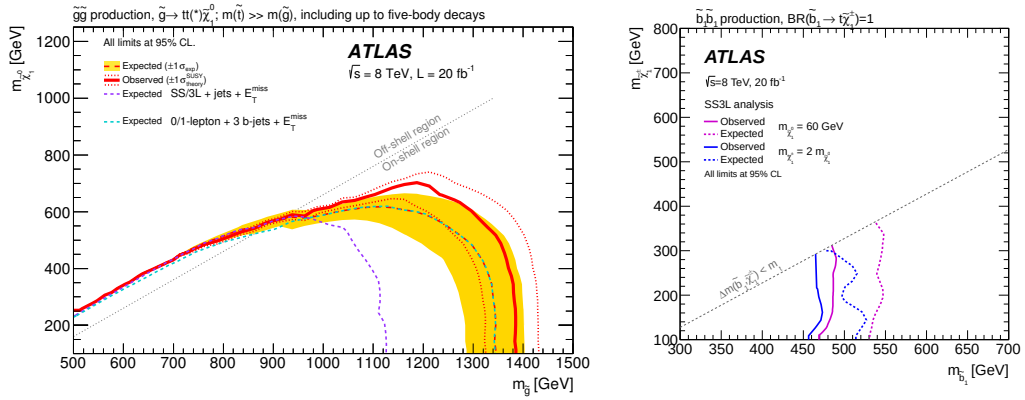

(a) (b)

Figure 5.2: Exclusion limits on the gluino-stop offshell [1] (left) and direct sbottom [2] (right) scenarios set by ATLAS with the 2012 dataset prior to the author's work.

a rather low acceptance due to the branching ratios of $W \to \ell\nu$ or $Z \to \ell\ell$. The exclusion limits obtained in run-1 (Fig. 5.3b) show again that the SS/3L+jets final state is very competitive to probe those models. This scenario is used as as benchmark to define the signal regions with ≥ 3 leptons and no b-jet.

The signal grid is built with variable gluino and $\tilde{\chi}_1^0$ masses; the $\tilde{\chi}_2^0$ mass is chosen half-way between the gluino and LSP masses, and the sleptons masses are also set equal and half-way between the $\tilde{\chi}_2^0$ and LSP masses. The $\tilde{\chi}_2^0$ may decay to any of the six "left-handed" sleptons ($\tilde{\ell}$, $\tilde{\nu}$) with equal probability. "Right-handed" sleptons are assumed heavy and do not participate to the decay.

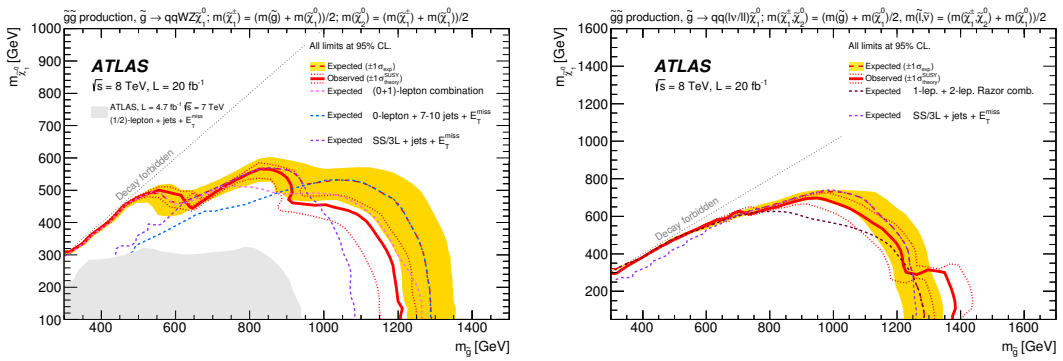

(a) (b)

Figure 5.3: Exclusion limits on scenarios featuring gluino pair production followed by two-step decays via heavy gauge bosons or sleptons, set by ATLAS with the 2012 dataset prior to the author's work [1].

Gluino pair production with gaugino-mediated two-step decay $\tilde{g} \to q\bar{q}'WZ\tilde{\chi}_1^0$

This scenario (Fig. 5.1c) features gluino pair-production with two-step decays via gauginos and W and Z bosons, $\tilde{g} \to q\bar{q}'\tilde{\chi}_1^\pm \to q\bar{q}'W\tilde{\chi}_2^0 \to q\bar{q}'WZ\tilde{\chi}_1^0$, mediated by generic heavy squarks of the first and second generations. The final state is made of two W and two Z bosons (possibly offshell), four additional jets and invisible particles (neutrinos and neutralinos). This generally leads to events with large jet multiplicities and a fair branching ratio for dileptonic final states. The exclusion limits obtained in run-1 indeed illustrate the competitiveness of the SS/3L+jets search (Fig. 5.3a) particularly the heavy-$\tilde{\chi}_1^0$ region of the phase space. This scenario is used as as benchmark to define the signal regions with many jets but none tagged as a b-jet.

The signal grid is built with variable gluino and $\tilde{\chi}_1^0$ masses, and the $\tilde{\chi}_1^\pm$ and $\tilde{\chi}_2^0$ masses are set such that the former lies half-way between the gluino and $\tilde{\chi}_1^0$ masses, and the latter half-way between $\tilde{\chi}_1^\pm$ and $\tilde{\chi}_1^0$ masses.

Sbottom pair production with one-step decay $\tilde{b}_1 \to t\tilde{\chi}_1^\pm$

In this scenario (Fig. 5.1e), bottom squarks are rather light and assumed to decay in a top quark and a chargino $\tilde{\chi}_1^\pm$, with a subsequent $\tilde{\chi}_1^\pm \to W^\pm\tilde{\chi}_1^0$ decay, providing complementarity to the mainstream search [3] which focuses on the channel $\tilde{b}_1 \to b\tilde{\chi}_1^0$. The final state resulting from the production of a $\tilde{b}_1\tilde{b}_1^*$ pair contains two top quarks, two W bosons and two neutralinos. While this final state may lead to various experimental signatures, the model was considered in Run-1 [1] only by the same-sign leptons and jets search, leading to the exclusion limits presented in Fig. 5.2. Signal events typically contain one or two b-tagged jets, therefore this scenario is used as benchmark to define the signal regions with ≥ 1 b-jet.

The model adopts a fixed chargino-neutralino mass difference of 100 GeV, therefore always allowing on-shell W bosons in the $\tilde{\chi}_1^\pm \to W\tilde{\chi}_1^0$ decay [1] Only pair production of the lightest sbottom is considered, followed by an exclusive decay in the aforementioned channel.

[1] A different chargino mass assumption is adopted in the current work compared to the Run-1 paper [1]. Fig. 5.2 is shown for illustration only. The reduced chargino-neutralino mass gap in the current analysis allows to study signal scenarios with heavy neutralinos, which were not considered previously.

Gluino pair production with stop-mediated decay $\tilde{g} \to t\bar{t}\tilde{\chi}_1^0$

In this scenario inspired by naturalness arguments, gluinos are coupling preferentially to stops which are lighter than the other squarks. Gluinos are however considered lighter than stops, and decay directly into a $t\bar{t}\tilde{\chi}_1^0$ triplet via a virtual stop (Fig. 5.1a). The pair production of gluinos leads to a final state containing four top quarks and two neutralinos. This characteristic final state is accessible through various experimental signatures, which is why this model is commonly used as a benchmark to compare analyses sensitivities. The searches performed with Run-1 data [1], summarized in Fig. 5.2a, showed that the same-sign leptons final state is competitive only at large neutralino mass. This region of the phase space is consequently given a particular attention in the choice of signal regions described further on. For instance, the region of phase-space with $\Delta m(\tilde{g}, \tilde{\chi}_1^0) < 2m_t$, where gluinos decay via one or two offshell top quarks, is only accessible for this analysis. In the signal samples referenced in this document, the mass of the lightest stop is fixed to 10 TeV and is mostly a $\widetilde{t}_R$ state. Only gluino pair production is considered, followed by an exclusive decay in the aforementioned channel. Signal events typically contain many b-tagged jets, therefore this scenario is used as benchmark to define the signal regions with ≥ 2 b-jets.

$\tilde{t}_1\tilde{t}_1^*$ with "three-same-sign leptons" signature

Inspired by Ref. [4], a simplified model featuring a stop pair-production with two-step decays via a neutralino $\tilde{\chi}_2^0$ and a chargino $\tilde{\chi}_1^\pm$ is added in this version of

the analysis, according to the decay illustrated on Fig. 5.1f:

$\tilde{t}_1 \to t\tilde{\chi}_2^0 \to t\tilde{\chi}_1^{\pm}W^{\mp} \to tW^{\pm}W^{\mp}\tilde{\chi}_1^0$.

This simplified model is a well-motivated representation of a pMSSM model. The lightest stop ($\tilde{t}_1$) is right-handed and $\tilde{\chi}_2^0$ is bino-like which leads to a large branching ratio in the decay $\tilde{t}_1 \to t\tilde{\chi}_2^0$. Furthermore, the decay $\tilde{\chi}_2^0 \to \tilde{\chi}_1^{\pm}W^{\mp}$ is also enhanced since $\tilde{\chi}_1^{\pm}$ is wino-like, as long as $\tilde{\chi}_1^{\pm}$ and $\tilde{\chi}_1^0$ are nearly mass degenerate and $m_{\tilde{\chi}_2^0} - m_{\tilde{\chi}_1^0} < m_H = 125$ GeV to suppress the decay $\tilde{\chi}_2^0 \to \tilde{\chi}_1^0 + H$ (the decay $\tilde{\chi}_2^0 \to \tilde{\chi}_1^0 + Z$ is suppressed). By respecting these conditions and evading the bottom squark limit shown in Fig. 5.2b, we consider a one-dimensional grid with a $\tilde{t}_1$ mass varying between 550 GeV and 800 GeV with a 50 GeV gap[2], a two body decay to an on-shell top quark and a $\tilde{\chi}_2^0$ which has a 100 GeV mass difference from $\tilde{\chi}_1^0$. The mass difference between the $\tilde{\chi}_1^{\pm}$ and $\tilde{\chi}_1^0$ is taken to be 500 MeV which is not excluded by the disappearing track analysis. In fact, this mass gap could easily be increased by introducing a small amount of higgsino mixing [5].

While the stop pair production is similar to the sbottom pair production in terms of kinematics, the stop pair production offers a unique topology that leads to three leptons of the same electric charge. This final state benefits from an extreme reduction of the SM background while maintaining a good signal acceptance which helps loosen the kinematic cuts to access a more compressed SUSY phase space. As a result, this scenario is complementary to the search for bottom squarks.

[2]Only the points at $\tilde{t}_1$ mass of 550 GeV are available at the moment.

Non-Universal Higgs Models

In references [6, 7, 8], theorists studied a complete two-extra-parameter non-universal Higgs model (NUHM2) that can have low fine tuning (natural) and predicts final state signatures that allow large background rejection while retaining high signal efficiency. The NUHM2 model allows the soft SUSY breaking masses of the Higgs multiplets, m_{H_u} and m_{H_d}, to be different from matter scalar masses (m_0) at the grand unification scale. The NUHM2 model is expected to form the effective theory for energies lower than m_{GUT} resulting from SU(5) or general SU(10) grand unified theories. The scalar mass m_0, the soft SUSY breaking gaugino mass $m_{1/2}$, the pseudoscalar Higgs boson mass m_A, the trilinear SUSY breaking parameter A_0, the weak scale ratio of Higgs field vacuum expectation values $\tan\beta$, and the superpotential Higgs mass μ are the free parameters. Both $m_{1/2}$ and μ are varied while the other parameters are fixed to $m_0 = 5$ TeV, $A_0 = -1.6m_0$, $\tan\beta = 15$, $m_A = 1$ TeV, and sign(μ)>0. These parameter choices lead directly to a Higgs mass of 125 GeV in accord with experiment. In this "radiatively-driven natural" SUSY approach, the higgsino is required to have mass below 200-300 GeV, the stop to have a mass below ∼3 TeV, and the gluino below ∼4 TeV. The model mainly involves gluino pair production with gluinos decaying predominantly to $t\bar{t}\tilde{\chi}_1^0$ and $tb\tilde{\chi}_1^{\pm}$, giving rise to final states with two same-sign leptons and $E_{\mathrm{T}}^{\mathrm{miss}}$. Table 5.1 shows the branching ratios of the dominant gluino decay modes for $m_{1/2} = 400$ GeV. Simulated NUHM2 signal samples with mass ($m_{1/2}$) values from 300-800 GeV and $\mu = 150$ GeV were generated where the

Decay	BR	Decay	BR
$t\bar{t}\chi_1^0$	0.13	$tb\chi_1^\pm$	0.45
$t\bar{t}\chi_2^0$	0.21	$tb\chi_2^\pm$	0.04
$t\bar{t}\chi_3^0$	0.13	-	-
$t\bar{t}\chi_4^0$	0.02	-	-
$t\bar{t}\chi_i^0$	0.49	$tb\chi_i^\pm$	0.49

Table 5.1: The dominant gluino decay modes for $m_{1/2} = 400$ GeV for the NUHM2 model.

gluino mass in this model is approximately $2.5 \times m_{1/2}$.

5.3 Dataset and Simulated Event Samples

5.3.1 Collision Data

The analysis uses pp–collisions data at $\sqrt{s} = 13$ TeV collected by the ATLAS detector during 2015 and 2016 with a peak instantaneous luminosity of $L = 1.4 \times 10^{34}$ cm^{-2}s^{-1}. The total integrated luminosity considered corresponds to 36.1 fb^{-1} (3.2 fb^{-1} in 2015 and 32.9 fb^{-1} in 2016) recorded after applying beam, detector, and data-quality requirements. The combined luminosity uncertainty for 2015 and 2016 is 3.2%, assuming partially correlated uncertainties in 2015 and 2016. The integrated luminosity was established following the same methodology as that detailed in Ref. [9], from a preliminary calibration of the luminosity scale

using a pair of x-y beam separation scans.

5.3.2 Simulated Event Samples

Monte Carlo (MC) simulated event samples are used to model the SUSY signal and SM backgrounds. The irreducible SM backgrounds refer to processes that lead to two same-sign and/or three "prompt" leptons where the prompt leptons are produced directly in the hard-scattering process, or in the subsequent decays of W, Z, H bosons or prompt τ leptons. The reducible backgrounds, mainly arising from $t\bar{t}$ and V+jets production , are estimated either from data or from MC simulation as described in Section 6.

Table 5.2 presents the event generator, parton shower, cross-section normalization, PDF set and the set of tuned parameters for the modelling of the parton shower, hadronization and underlying event. Apart from the MC samples produced by the SHERPA generator, all MC samples used the EVTGEN v1.2.0 program [10] to model the properties of bottom and charm hadron decays.

The MC samples were processed through either a full ATLAS detector simulation [23] based on GEANT4 [24] or a fast simulation using a parameterization of the calorimeter response and GEANT4 for the ID and MS [25], and are reconstructed in the same manner as the data. All simulated samples are generated with a range of minimum-bias interactions using PYTHIA 8 [12] with the MSTW2008LO PDF set [26] and the A2 tune overlaid on the hard-scattering event to account for the multiple pp interactions in the same bunch crossing (in-time pileup) and neighbouring bunch crossing (out-of-time pileup). The distribution of the average

Physics process	Event generator	Parton shower	Cross-section normalization	PDF set	Set of tuned parameters
Signal	aMC@NLO 2.2.3 [11]	Pythia 8.186 [12]	NLO+NLL	NNPDF2.3LO [13]	A14 [14]
$t\bar{t}+X$					
$t\bar{t}W$, $t\bar{t}Z/\gamma^*$	aMC@NLO 2.2.2	Pythia 8.186	NLO [15]	NNPDF2.3LO	A14
$t\bar{t}H$	aMC@NLO 2.3.2	Pythia 8.186	NLO [15]	NNPDF2.3LO	A14
$4t$	aMC@NLO 2.2.2	Pythia 8.186	NLO [11]	NNPDF2.3LO	A14
Diboson					
ZZ, WZ	Sherpa 2.2.1 [16]	Sherpa 2.2.1	NLO [17]	NNPDF2.3LO	Sherpa default
Other (inc. $W^{\pm}W^{\pm}$)	Sherpa 2.1.1	Sherpa 2.1.1	NLO [17]	CT10 [18]	Sherpa default
Rare					
$t\bar{t}WW$, $t\bar{t}WZ$	aMC@NLO 2.2.2	Pythia 8.186	NLO [11]	NNPDF2.3LO	A14
tZ, tWZ, $tt\bar{t}$	aMC@NLO 2.2.2	Pythia 8.186	LO	NNPDF2.3LO	A14
WH, ZH	aMC@NLO 2.2.2	Pythia 8.186	NLO [19]	NNPDF2.3LO	A14
Triboson	Sherpa 2.1.1	Sherpa 2.1.1	NLO [17]	CT10	Sherpa default
Irreducible					
$t\bar{t}$	Powheg-Box	Pythia 6.428	NNLO+NNLL [20]	CT10	PERUGIA2012 (P2012) [21]
W+Jets, Z+Jets	Powheg-Box	Pythia 8.186	NNLO [20]	CT10	AZNLO[22]

Table 5.2: Simulated signal and background event samples: the corresponding event generator, parton shower, cross-section normalization, PDF set and set of tuned parameters are shown for each sample. Because of their very small contribution to the signal-region background estimate, $t\bar{t}WW$, $t\bar{t}WZ$, tZ, tWZ, $tt\bar{t}$, WH, ZH and triboson are summed and labelled "rare" in the following.

number of interactions per bunch crossing $\langle\mu\rangle$ ranges from 0.5 to 39.5, with a profile set as an estimate of the combined 2015+2016 data $\langle\mu\rangle$ profile. With larger luminosity collected during this year and the μ distribution in data being closer to that in the MC profile, the simulated samples are reweighted to reproduce the observed distribution of the average number of collisions per bunch crossing (μ).

Background process simulation

The two dominant irreducible background processes are $t\bar{t}V$ (with V being a W or Z/γ^* boson) and diboson production with final states of four charged leptons ℓ,[3] three charged leptons and one neutrino, or two same-sign charged leptons and two neutrinos.

The production of a $t\bar{t}V$ constitutes the main source of background with prompt same-sign leptons for event selections including b-jets. Simulated events for these processes were generated at NLO with aMC@NLO v2.2.2 [11] interfaced to Pythia 8, with up to two (ttW) or one ($ttZ^{(*)}$) extra parton included in the matrix elements [27]. The samples are normalised to the inclusive process NLO cross-section using appropriate k-factors [11].

The production of multiple W, Z bosons decaying leptonically constitutes the main source of background with prompt same-sign leptons for event selections vetoing b-jets. Diboson processes with four charged leptons, three charged leptons and one neutrino, or two charged leptons and two neutrinos were simulated at NLO using the Sherpa 2.2.1 generator [16], as described in detail in Ref. [17]. The main samples simulate $qq \to VV \to$ leptons production including the doubly resonant WZ and ZZ processes, non-resonant contributions as well as Higgs-mediated contributions, and their interferences; up to three extra partons were included (at LO) in the matrix elements. Simulated events for the $W^{\pm}W^{\pm}jj$ process (including non-resonant contributions) were produced at LO with up

[3] All lepton flavours are included here and τ leptons subsequently decay leptonically or hadronically.

to one extra parton, separately for QCD-induced ($\mathcal{O}(\alpha_{\text{em}}^4)$) and VBS-induced ($\mathcal{O}(\alpha_{\text{em}}^6)$) production – the interferences being neglected. Additional samples for VBS-induced $qq \to 3\ell\nu jj$ and $qq \to 4\ell$ and loop-induced $gg \to WZ^{(*)}/ZZ^{(*)}$ processes were also produced with the same configuration. The samples generated at NLO are directly normalized to the cross-sections provided by the generator.

Production of a Higgs boson in association with a $t\bar{t}$ pair is simulated using aMC@NLO [11] (in MadGraph v2.2.2) interfaced to Herwig 2.7.1 [28]. The UEEE5 underlying-event tune is used together with the CTEQ6L1 [29] (matrix element) and CT10 [18] (parton shower) PDF sets. Simulated samples of SM Higgs boson production in association with a W or Z boson are produced with Pythia 8.186, using the A14 tune and the NNPDF23LO PDF set. Events are normalised with cross-sections calculated at NLO [19].

MadGraph v2.2.2 [30] is used to simulate the $t\bar{t}WW$, tZ, $t\bar{t}t\bar{t}$ and $t\bar{t}t$ processes, and the generator cross-section is used for tZ and $t\bar{t}t$. MadGraph interfaced to Pythia 8 is used to generate $t\bar{t}WZ$ processes, and appropriate k-factors are taken from [11]. aMC@NLO interfaced to Pythia 8 is used for the generation of the tWZ process, with an alternative sample generated with aMC@NLO interfaced to Herwig used to evaluate the parton shower uncertainty. Fully leptonic triboson processes (WWW, WWZ, WZZ and ZZZ) with up to six charged leptons are simulated using Sherpa v2.1.1 and described in Ref. [17]. The 4ℓ and $2\ell + 2\nu$ processes are calculated at next-to-leading order (NLO) for up to one additional parton; final states with two and three additional partons are calculated at leading order (LO). The $WWZ \to 4\ell + 2\nu$ or $2\ell + 4\nu$ processes are calculated at LO with

up to two additional partons. The $WWW/WZZ \to 3\ell + 3\nu$, $WZZ \to 5\ell + 1\nu$, $ZZZ \to 6\ell + 0\nu$, $4\ell + 2\nu$ or $2\ell + 4\nu$ processes are calculated is calculated at NLO with up to two extra partons at LO. The CT10 [18] parton distribution function (PDF) set is used for all SHERPA samples in conjunction with a dedicated tuning of the parton shower parameters developed by the SHERPA authors. The generator cross-sections (at NLO for most of the processes) are used when normalising these backgrounds.

Double parton scattering (DPS) occurs when two partons interact simultaneously in a proton-proton collision leading to two hard scattering processes overlapping in a detector event. Accordingly, two single W production processes can lead to a $W^{\pm} + W^{\pm}$ final state via DPS. This background is expected to have a negligeable contribution to signal regions with high jet multiplicities. To estimate a conservative upper bound on cross-section for WW events which might arise from DPS, a standard ansatz is adopted: in this, for a collision in which a hard process (X) occurs, the probability that an additional (distinguishable) process (Y) occurs is parametrized as:

$$\sigma_{XY}^{DPS} = \sigma_X \sigma_Y / \sigma_{eff} \tag{5.1}$$

where σ_X is the production cross section of the hard process X and σ_{eff} (effective area parameter) parameterizes the double-parton interaction part of the production cross section for the composite system (X+Y). A value of σ_{eff} is 10-20 mb is assumed in this study (as obtained from 7 TeV measurements, and with no observed dependence on $\sqrt{s}$), and it is independent on the processes involved. For

the case of $W^{\pm} + W^{\pm}$ production:

$$\sigma^{DPS}_{W^{\pm}W^{\pm}} = \frac{\sigma_{W^+}\sigma_{W^+} + \sigma_{W^-}\sigma_{W^-} + 2\sigma_{W^+}\sigma_{W^-}}{\sigma_{eff}} \simeq 0.19 - 0.38 \text{ pb.} \tag{5.2}$$

After the application of the SR criteria, only 4 raw MC events in the DPS $WW \to \ell\nu\ell\nu$ remain. Table 5.3 shows the expected contribution in the SRs where some MC event survives all the cuts. The ranges quoted in the tables reflect the range in the predicted $\sigma^{DPS}_{W^{\pm}W^{\pm}}$ cross-section above, as well as the combinatorics for scaling the jet multiplicity[4]. Due to the large uncertainties involved in these estimates, some of them difficult to quantify (such as the modelling of DPS by Pythia at LO), the contribution from this background is not included in the final SR background estimates. Note that the estimated DPS contribution is typically much smaller than the uncertainty on the total background for the SRs.

Table 5.3: Number of raw MC events and its equivalent for 36.1 fb^{-1}with and without the correction as a function of the jet multiplicity. Only the SRs where at least one MC event passes all the cuts are shown.

SR	Raw MC evts	Without N_{jet} correction	With N_{jet} correction
Rpc2L0bS	2	0.016-0.033	0.09-0.38
Rpc2L0bH	1	0.006-0.012	0.05-0.17

Table 5.4: Signal cross-sections [pb] and related uncertainties [%] for scenarios featuring $\tilde{g}\tilde{g}$ (top table) or $\tilde{b}_1\tilde{b}_1^*$ (bottom table) production, as a function of the pair-produced superpartner mass, reproduced from Ref. [31].

Gluino mass (GeV)	500	550	600	650	700
Cross section (pb)	$27.4 \pm 14\%$	$15.6 \pm 14\%$	$9.20 \pm 14\%$	$5.60 \pm 14\%$	$3.53 \pm 14\%$
750	800	850	900	950	1000
$2.27 \pm 14\%$	$1.49 \pm 15\%$	$0.996 \pm 15\%$	$0.677 \pm 16\%$	$0.466 \pm 16\%$	$0.325 \pm 17\%$
1050	1100	1150	1200	1250	1300
$0.229 \pm 17\%$	$0.163 \pm 18\%$	$0.118 \pm 18\%$	$0.0856 \pm 18\%$	$0.0627 \pm 19\%$	$0.0461 \pm 20\%$
1350	1400	1450	1500	1550	1600
$0.0340 \pm 20\%$	$0.0253 \pm 21\%$	$0.0189 \pm 22\%$	$0.0142 \pm 23\%$	$0.0107 \pm 23\%$	$0.00810 \pm 24\%$

Sbottom mass (GeV)	400	450	500	550
Cross section (pb)	$1.84 \pm 14\%$	$0.948 \pm 13\%$	$0.518 \pm 13\%$	$0.296 \pm 13\%$
600	650	700	750	800
$0.175 \pm 13\%$	$0.107 \pm 13\%$	$0.0670 \pm 13\%$	$0.0431 \pm 14\%$	$0.0283 \pm 14\%$

Signal cross-sections and simulations

The signal processes are generated from leading order (LO) matrix elements with up to two extra partons (only one for the grid featuring slepton-mediated gluino decays), using the MADGRAPH v5.2.2.3 generator [11] interfaced to PYTHIA 8.186 [12] with the *ATLAS 14* tune [14] for the modelling of the SUSY decay chain, parton showering, hadronisation and the description of the underlying event. Parton luminosities are provided by the NNPDF23LO [32] set of parton

[4]For instance, a DPS event with 6 jets can be due to the overlap of two events with 6+0 jets, or 5+1, 4+2 or 3+3 jets. All possible combinations are considered and the range quoted in the table shows the combinations leading to the smallest and largest correction factors.

distribution functions. Jet-parton matching is realized following the CKKW-L prescription [33], with a matching scale set to one quarter of the pair-produced superpartner mass.

The signal samples are normalised to the next-to-next-to-leading order cross-section from Ref. [31] including the resummation of soft gluon emission at next-to-next-to-leading-logarithmic accuracy (NLO+NLL), as detailed in Ref. [34]; some of these cross-sections are shown for illustration in Table 5.4.

Cross-section uncertainties are also taken from Ref. [31] as well, and include contributions from varied normalization and factorization scales, as well as PDF uncertainties. They typically vary between 15 and 25%. We do not consider any source of uncertainties on signal acceptance, experience having shown that these are generally smaller than the uncertainties on the inclusive production cross-section.

5.4 Event Selection

5.5 Signal Regions

Chapter 6

Data-driven Background Estimation Techniques

6.1 The problem of fakes

6.2 Common processes for faking leptons

6.3 The Monte Carlo Template Method

6.4 Matrix Method

Chapter 7

Background Estimation

7.1 Overview

7.2 Irreducible Backgrounds

7.3 Reducible Backgrounds

Chapter 8

Systematic uncertainties

8.1 Theretical Uncertainties

8.2 Experimental Uncertainties

Chapter 9

Statistical Treatment

Chapter 10

Results and Interpretation

Chapter 11

Conclusions

Appendix A

Auxiliary material

I am referencing the first thing [35].

References

[1] ATLAS Collaboration, JHEP **10** (2015) 054, arXiv:1507.05525 [hep-ex].

[2] ATLAS Collaboration, Eur. Phys. J. C **75** (2015) 510, arXiv:1506.08616 [hep-ex].

[3] ATLAS Collaboration, Atlas-conf-2015-066, https://cds.cern.ch/record/2114833.

[4] P. Huang, A. Ismail, I. Low, and C. E. M. Wagner, Phys. Rev. D **92** (2015) 075035, arXiv:1507.01601 [hep-ph].

[5] ATLAS Collaboration, Phys. Rev. **D88** (2013).

[6] H. Baer, V. Barger, P. Huang, D. Mickelson, A. Mustafayev, W. Sreethawong, and X. Tata, JHEP **12** (2013) 013, arXiv:1310.4858 [hep-ph], [Erratum: JHEP06,053(2015)].

[7] H. Baer, V. Barger, P. Huang, D. Mickelson, A. Mustafayev, W. Sreethawong, and X. Tata, Phys. Rev. Lett. **110** (2013) 151801, arXiv:1302.5816 [hep-ph].

[8] H. Baer, V. Barger, M. Savoy, and X. Tata, Phys. Rev. **D94** (2016) 035025, arXiv:1604.07438 [hep-ph].

[9] ATLAS Collaboration, ATLAS Collaboration, Eur. Phys. J. C **76** (2016) 653, arXiv:1608.03953 [hep-ex].

[10] D. J. Lange, Nucl. Instrum. Meth. A **462** (2001) 152.

[11] J. Alwall, R. Frederix, S. Frixione, V. Hirschi, F. Maltoni, O. Mattelaer, H. S. Shao, T. Stelzer, P. Torrielli, and M. Zaro, JHEP **07** (2014) 079, arXiv:1405.0301 [hep-ph].

[12] T. Sjöstrand, S. Mrenna, and P. Skands, Comput. Phys. Commun. **178** (2008) 852–867, arXiv:0710.3820 [hep-ph].

[13] R. D. Ball et al., Nucl. Phys. B **867** (2013) 244–289, arXiv:1207.1303 [hep-ph].

[14] ATLAS Collaboration, Atl-phys-pub-2014-021, https://cds.cern.ch/record/1966419.

[15] LHC Higgs Cross Section Working Group Collaboration, D. de Florian et al., arXiv:1610.07922 [hep-ph].

[16] T. Gleisberg et al., JHEP **02** (2009) 007, arXiv:0811.4622 [hep-ph].

[17] ATLAS Collaboration, Atl-phys-pub-2016-002, http://cds.cern.ch/record/2119986.

[18] H.-L. Lai et al., Phys. Rev. D **82** (2010) 074024, arXiv:1007.2241 [hep-ph].

[19] LHC Higgs Cross Section Working Group Collaboration, LHC Higgs Cross Section Working Group, arXiv:1201.3084 [hep-ph].

[20] M. Czakon and A. Mitov, Comput. Phys. Commun. **185** (2014) 2930, arXiv:1112.5675 [hep-ph].

[21] P. Skands, Phys. Rev. D **82** (2010) 074018, arXiv:1005.3457 [hep-ph].

[22] ATLAS Collaboration, JHEP **2014** (2014) 55, arXiv:1406.3660 [hep-ex].

[23] ATLAS Collaboration, G. Aad et al., Eur.Phys.J. **C70** (2010) 823–874, arXiv:1005.4568 [physics.ins-det].

[24] GEANT4 Collaboration, S. Agostinelli et al., Nucl. Instrum. Meth. A **506** (2003) 250–303.

[25] ATLAS Collaboration, ATL-PHYS-PUB-2010-013, http://cds.cern.ch/record/1300517.

[26] A. Sherstnev and R. Thorne, Eur. Phys. J. C **55** (2008) 553–575, arXiv:0711.2473 [hep-ph].

[27] ATLAS Collaboration, Atl-phys-pub-2016-005, http://cds.cern.ch/record/2120826.

[28] G. Corcella et al., JHEP **01** (2001) 010, arXiv:hep-ph/0011363.

[29] J. Pumplin et al., JHEP **07** (2002) 012, arXiv:hep-ph/0201195.

[30] J. Alwall, M. Herquet, F. Maltoni, O. Mattelaer, and T. Stelzer, JHEP **06** (2011) 128, arXiv:1106.0522 [hep-ph].

[31] LHC SUSY Cross Section Working Group, 2015, https://twiki.cern.ch/twiki/bin/view/LHCPhysics/SUSYCrossSections.

[32] S. Carrazza, S. Forte, and J. Rojo, *Parton distributions and event generators*, pp. , 89–96. 2013. arXiv:1311.5887 [hep-ph].

[33] L. Lönnblad and S. Prestel, JHEP **03** (2012) 019, arXiv:1109.4829 [hep-ph].

[34] C. Borschensky et al., Eur. Phys. J. C **74** (2014) 3174, arXiv:1407.5066 [hep-ph].

[35] ATLAS Collaboration, JINST **3** (2008) S08003.